# High-frequency restoration of surface seismic data

SATINDER CHOPRA, VLADIMIR ALEXEEV, and VASUDHAVEN SUDHAKAR, Core Laboratories Reservoir Technologies Division, Calgary, Alberta, Canada

Often we come across examples in which the initial processing of a 3D seismic volume results in interpretations that are geologically suspect—e.g., cases involving complex faulted patterns or subtle stratigraphic plays. Similarly, postmortem analysis may cite small fault displacements or obscure seismic data as reasons for dry wells. In such cases, the usual practice is to create a new version of the 3D volume with some target-oriented processing to improve imaging in the zone of interest that will, in turn, lead to more accurate interpretation. This helps in some cases, but in others some questions remain unresolved.

In the latter, more often than not, more accurate stratigraphic interpretation is needed but the available bandwidth of the data is inadequate to image or resolve the thickness of many thin targets seen in wells.

This can be addressed by having data of reasonable quality and augmenting it by some frequency restoration procedure that improves the vertical resolution. Frequency restoration is necessary because seismic waves propagating in the subsurface are attenuated and this phenomenon is frequency dependent—higher frequencies are absorbed more rapidly than lower frequencies. Consequently, the highest frequency recovered on most seismic data is usually about 80 Hz. This article describes a new method for restoring high frequencies within the seismic bandwidth that is based on the frequency decay experienced at different VSP depth levels in a well.

**Restoring high frequencies in surface seismic.** It is well known that VSP data contain higher frequencies than surface seismic data because the energy recorded by VSP traverses the unconsolidated weathering zone just once. Figure 1, which shows sectional amplitude spectra computed for a profile through spatially coincident 3D seismic and 3D VSP volumes, confirm this observation. The frequency content of the surface seismic data extends to 60-65 Hz but it reaches 90 Hz in the 3D VSP data.

The method we describe, high frequency restoration (HFR), analyzes the frequency decay of direct arrivals at different VSP depth levels in a well and then compensates the surface seismic data for that decay.

Figure 2 shows the separated downgoing VSP wavefield. Careful examination of wavelets in the highlighted zone indicates the decrease in the frequency levels from the shallow to the deeper levels. The amplitude spectra (Figure 3) show the decrease in amplitude of the different frequency components between the shallow depth level (222.2 m) and a deeper depth level (1228 m).

For the VSP downgoing signals (Figure 2), the ratio of the change in trace frequency amplitudes at successive depths quantifies the decay of frequency components between those observation points. The change in the trace amplitudes and the length of the wavelet on the first arrivals at successive depth levels is used to estimate the change in the frequency components. An inverse operator (in time domain) is then designed to compensate for that difference. For successive depth levels, a suite of such operators is generated.

For example, consider zero-offset VSP data recorded at borehole depths $z_1, z_2, z_3, \ldots, z_n$. After separation of the component wavefields (downgoing, upgoing, PS, tube waves, etc.), let $u_i(t)$ indicate the downgoing wavefield amplitude at the $i^{th}$ receiver, which can be considered the incident direct arrival. It is then possible to determine the change in this wavelet in terms of frequency from one depth level to the next.

We can write

$$u_i(t) = p_i(t) * u_1(t) \quad (1)$$

where operator $p_i(t)$ describes the influence of the subsurface on the wavelet as it propagates from point $z_1$ to $z_i$.

The inverse operator $L_i = P_i^{-1} = \{l_i(t)\}$, that would restore the attenuated frequency amplitudes, can be written

$$u_1(t) = l_i(t) * u_i(t) \quad (2)$$

This equation can be solved in the time or frequency domain.

In the time domain, equation 2 can be solved by the least squares method, which leads to the Wiener equation:

$$\mathbf{Al = b} \quad (3)$$

where A is a matrix made from an autocorrelation function for $u_i(t)$, $l = (l(t_1), l(t_2), \ldots l(t_n))$, and $b = (b_1, b_2, \ldots, b_n)$ is the crosscorrelation function for $u_1(t)$ and $u_i(t)$.

To solve system 3, the well known method of Levinson can be used.

After a Fourier transform into the frequency domain, we obtain

$$U_1(\omega) = L_i(\omega)\, U_i(\omega) \quad (4)$$

where $U(\omega)$ is Fourier transform (complex spectrum) of $u(t)$.

From equation 4 it follows that

$$L_i(\omega) = U_1(\omega)/U_i(\omega) = U_1(\omega)U_i^*(\omega)/|U_i(\omega)|^2 \quad (5)$$

Since the real data contain noise as well as signal, instead of equation 5 we may use

$$L_i(\omega) = U_1(\omega)/U_i(\omega) = U_1(\omega)U_i^*(\omega)/[|U_i(\omega)|^2 + \alpha^2] \quad (6)$$

where $\alpha$ is the noise level.

**Application to seismic data.** First the aligned VSP upgoing wavefield is visually correlated with the seismic section so that each depth level point is seen in terms of two-way time where the predetermined operators need to be applied (Figure 4). The left side of Figure 4 shows the subsurface stratigraphy and the different logs tied (in depth) to the upgoing VSP wavefield. A good correlation here is essential for the accuracy of the correction we are attempting to apply. The right side shows the VSP corridor stack (in time) correlated with


AUGUST 2003 THE LEADING EDGE 0000

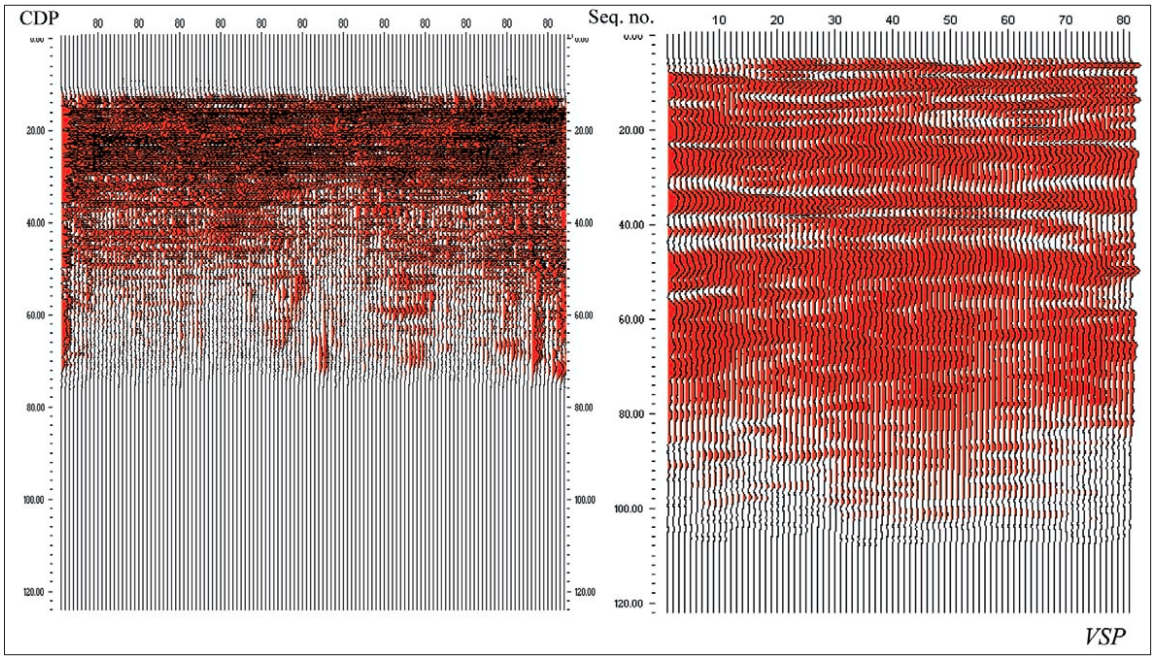


***Figure 1.*** *Sectional amplitude spectra of a profile from surface seismic (left), and 3D VSP (right). Vertical axis is frequency.*

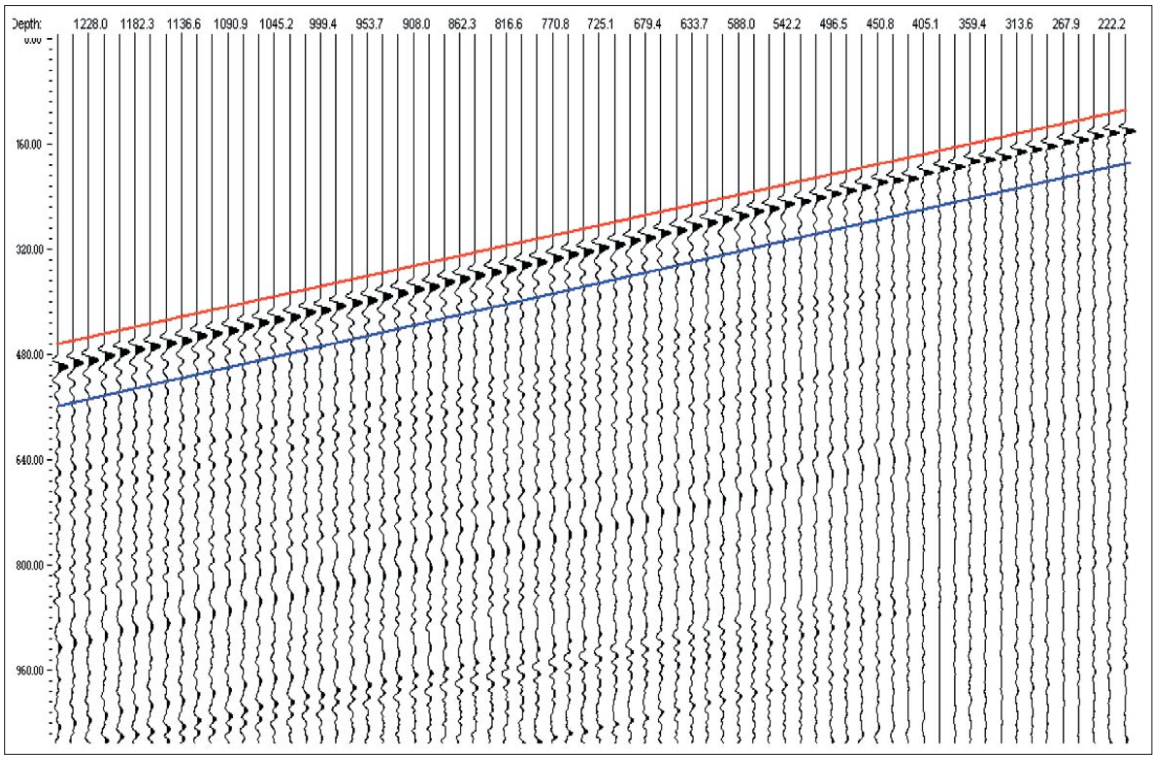


***Figure 2.*** *Downgoing wavefield obtained after separation of component wavefields from the VSP total wavefield for well 1.*

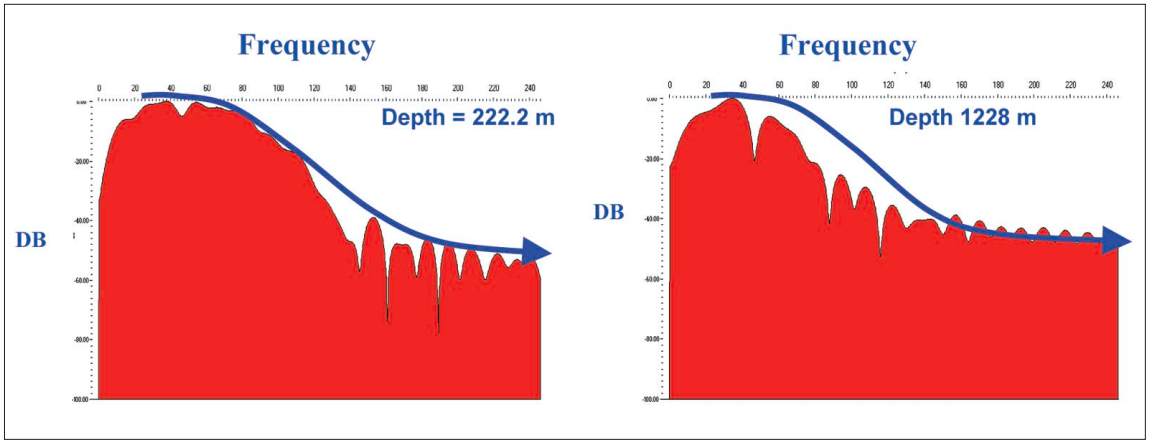


***Figure 3.*** *Amplitude spectra at a shallow and a deep depth level.*

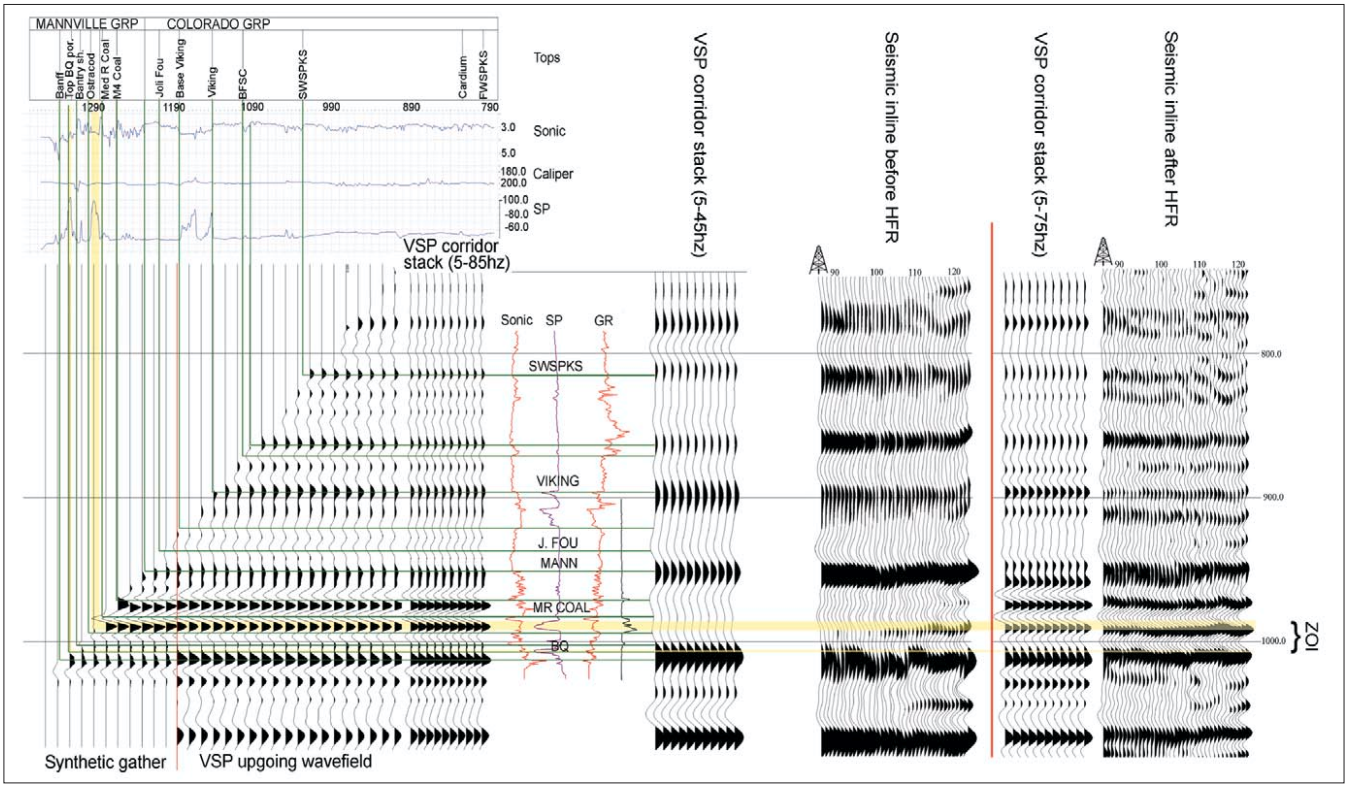


***Figure 4.*** *Correlation of stratigraphy, VSP upgoing wavefield, well logs, VSP corridor stack, and surface seismic data.*

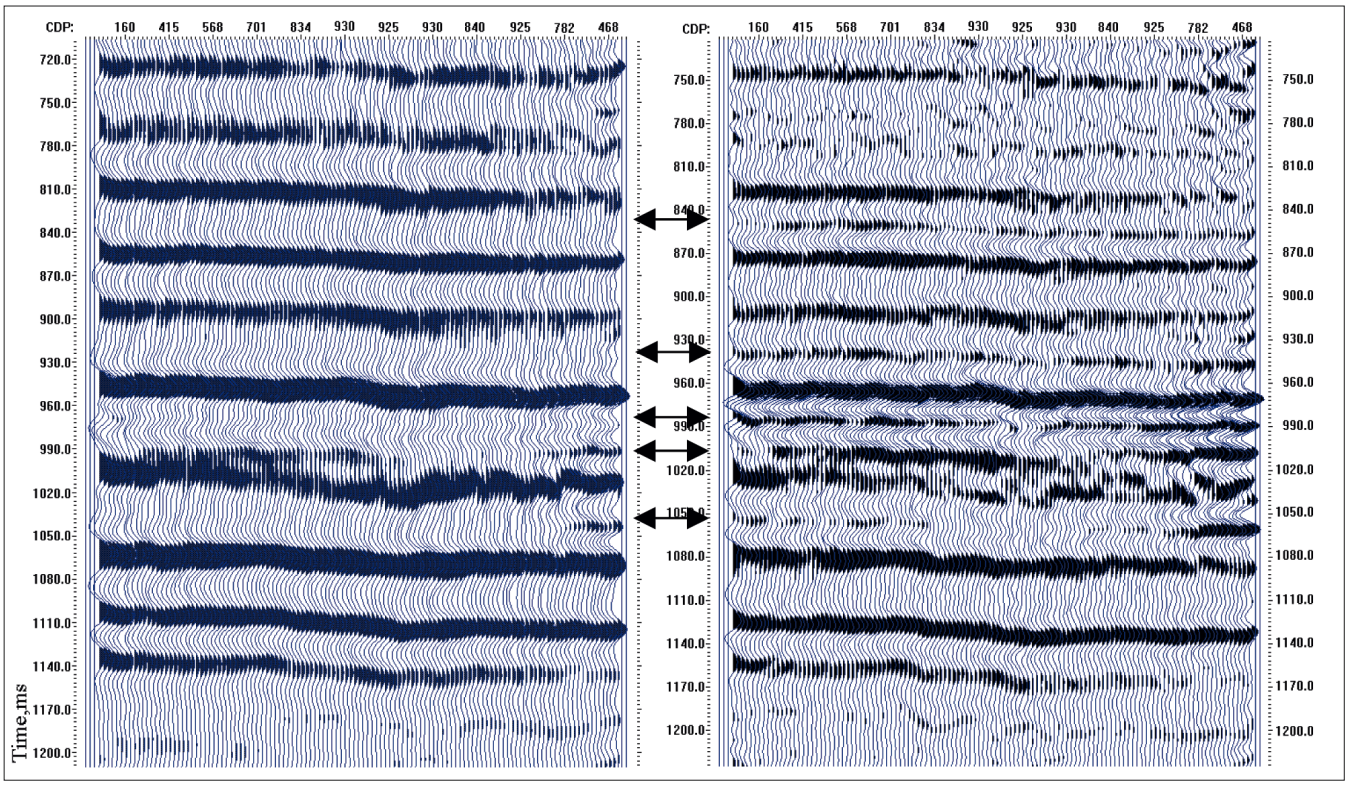


***Figure 5.*** *Seismic inline 85 extracted out of a 3D seismic volume before (left) and after (right) HFR.*

logs, a filtered version of the corridor stack, and the seismic section. The green lines indicate the depth-to-time matching of individual formation tops seen on the logs and upgoing wavefield (in depth) with the surface seismic data. This fixes the VSP upgoing wavefield extent or spread on the seismic. The first operator corresponding to the first depth level is now assigned a starting time and so, in this way, each determined operator has a corresponding time node point application on the seismic. Thereafter, the filter application is run (as convolution in time domain) on the seismic data. As operators are applied continuously to the stacked data, windowing is avoided. Application of these inverse operators on surface seismic data enhance the frequency bandwidth by restoring the attenuated frequency components.

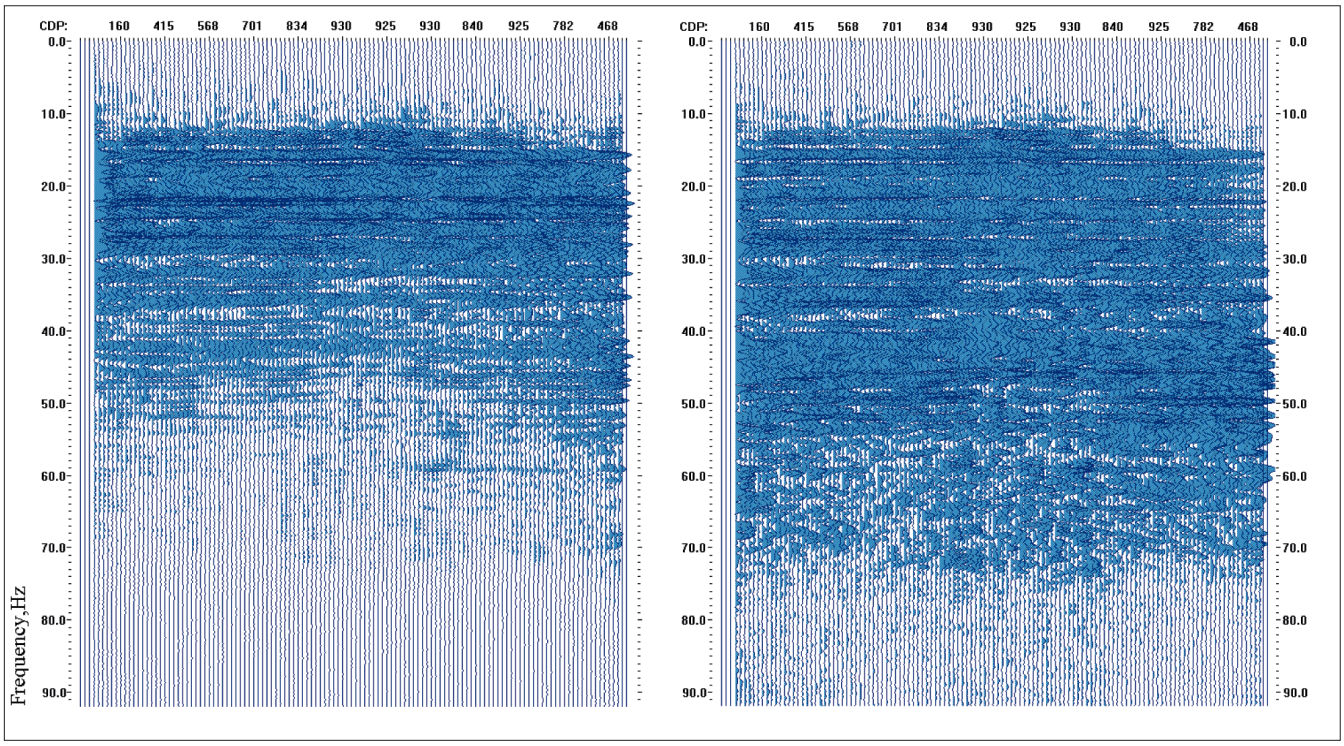


***Figure 6.*** *Sectional amplitude spectra for seismic inline 85 indicates the extent of frequency enhancement.*

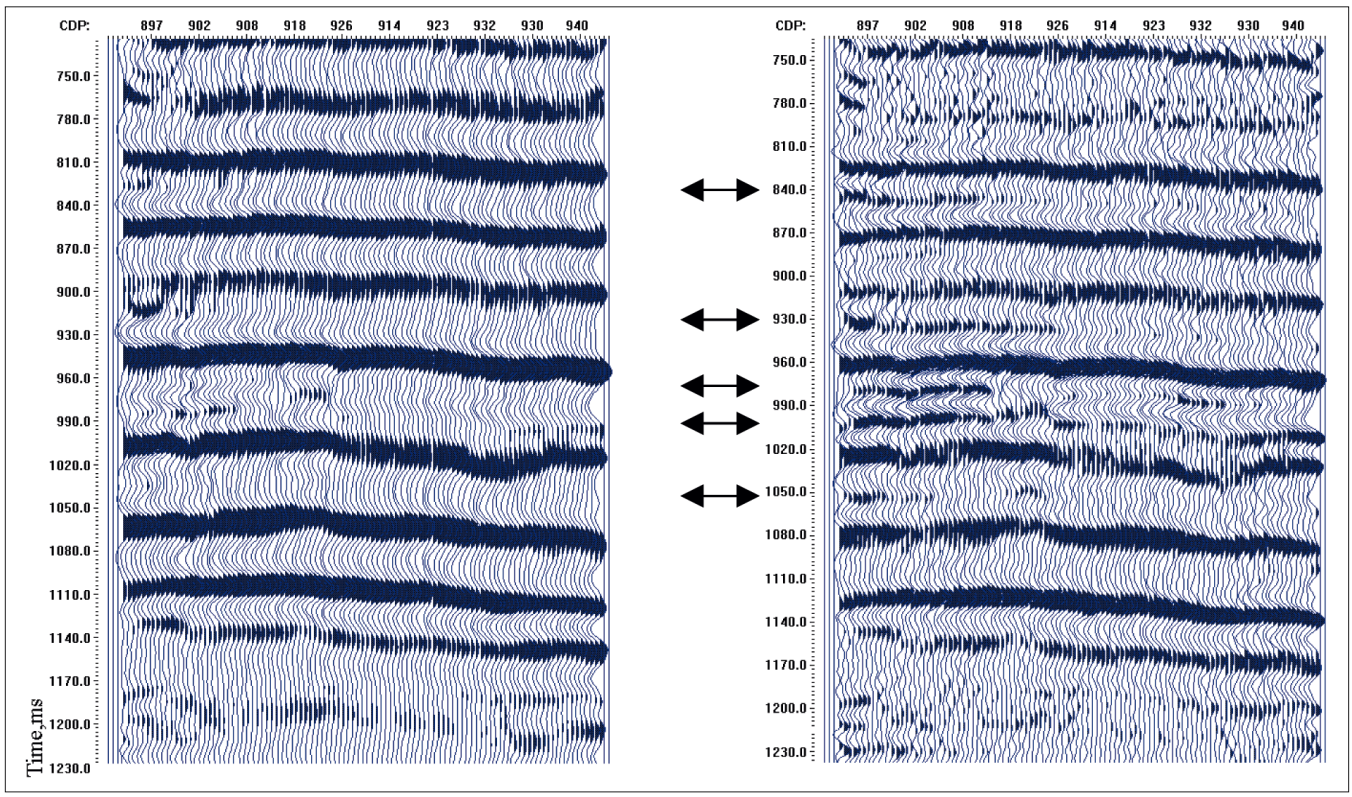


***Figure 7.*** *Seismic crossline 72 before (left) and after (right) HFR.*

A 3D VSP and a coincident 3D surface seismic survey were recorded around well 8-20 in the Hanna area of central Alberta, targeting the Lower Mannville formation (Chopra et al., 2002). The well encountered a gross Lower Mannville interval 20.5 m thick and thicker than in adjacent wells 6-20 (11.5 m) and 8-21 (7 m). The 3D seismic programs (surface and VSP) were recorded to assist in defining sand presence and porosity development in the Lower Mannville interval between 1300 and 1350 m. The objectives for the 3D VSP recording were to (a) tie the seismic reflections to lithology and stratigraphic boundaries; (b) obtain a high frequency image around the borehole (the fixed receiver array and its proximity to the reservoir are expected to improve image quality); and (c) obtain an improved subsurface velocity model.

HFR was run on the seismic data. Figure 5 shows a segment of seismic inline 85 with and without HFR. Notice the

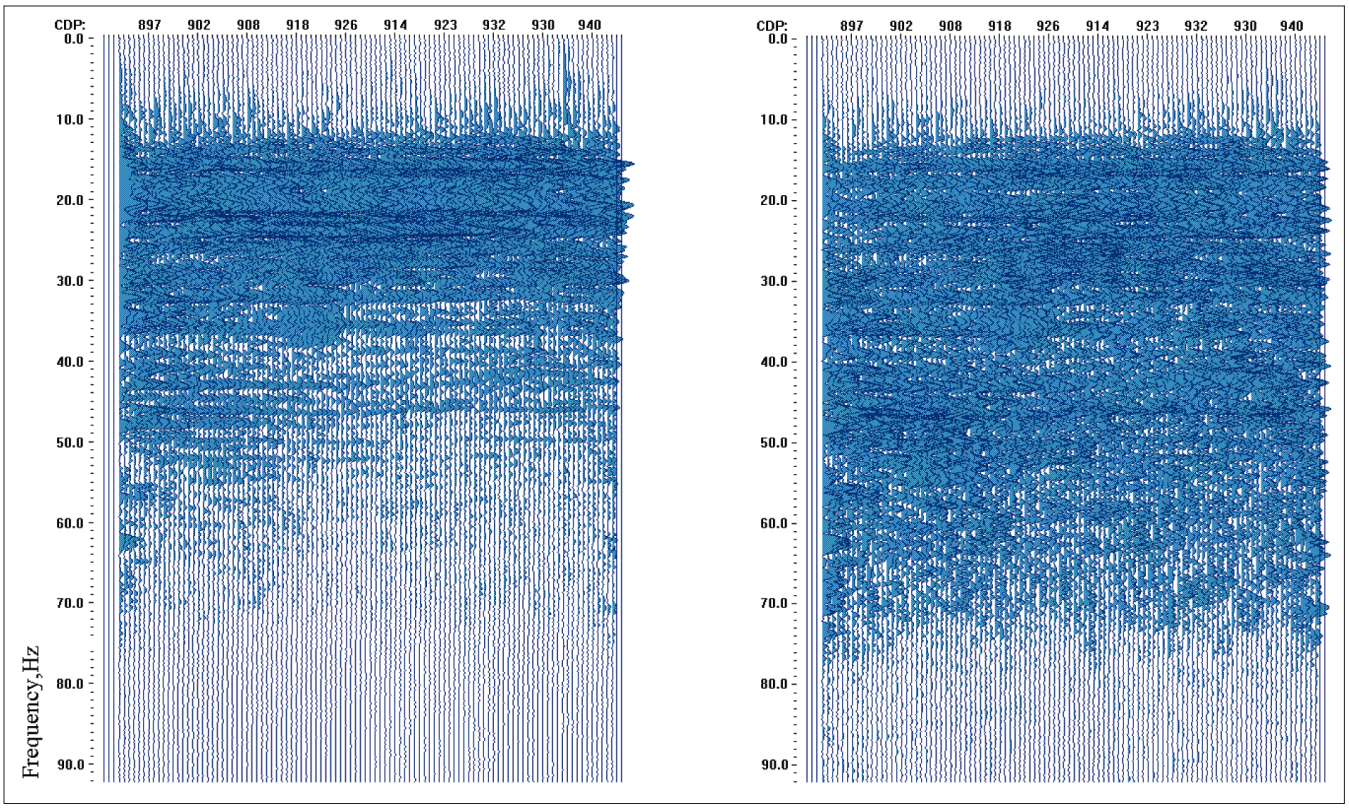


***Figure 8.*** *Sectional amplitude spectra for seismic crossline 72 before (left) and after (right) HFR.*

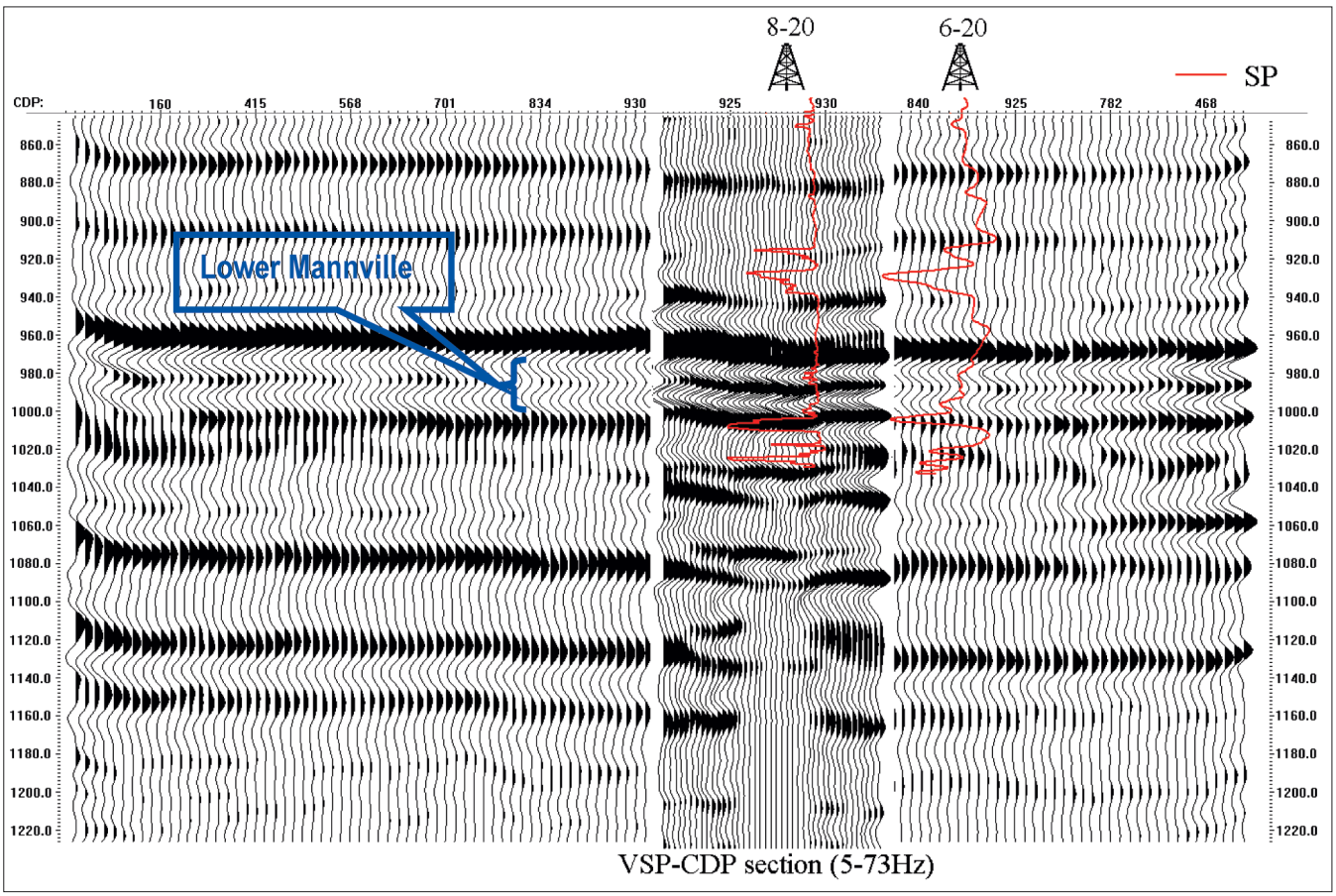


***Figure 9.*** *Overlay of a 3D VSP vertical plane and seismic (inline 85) after HFR.*

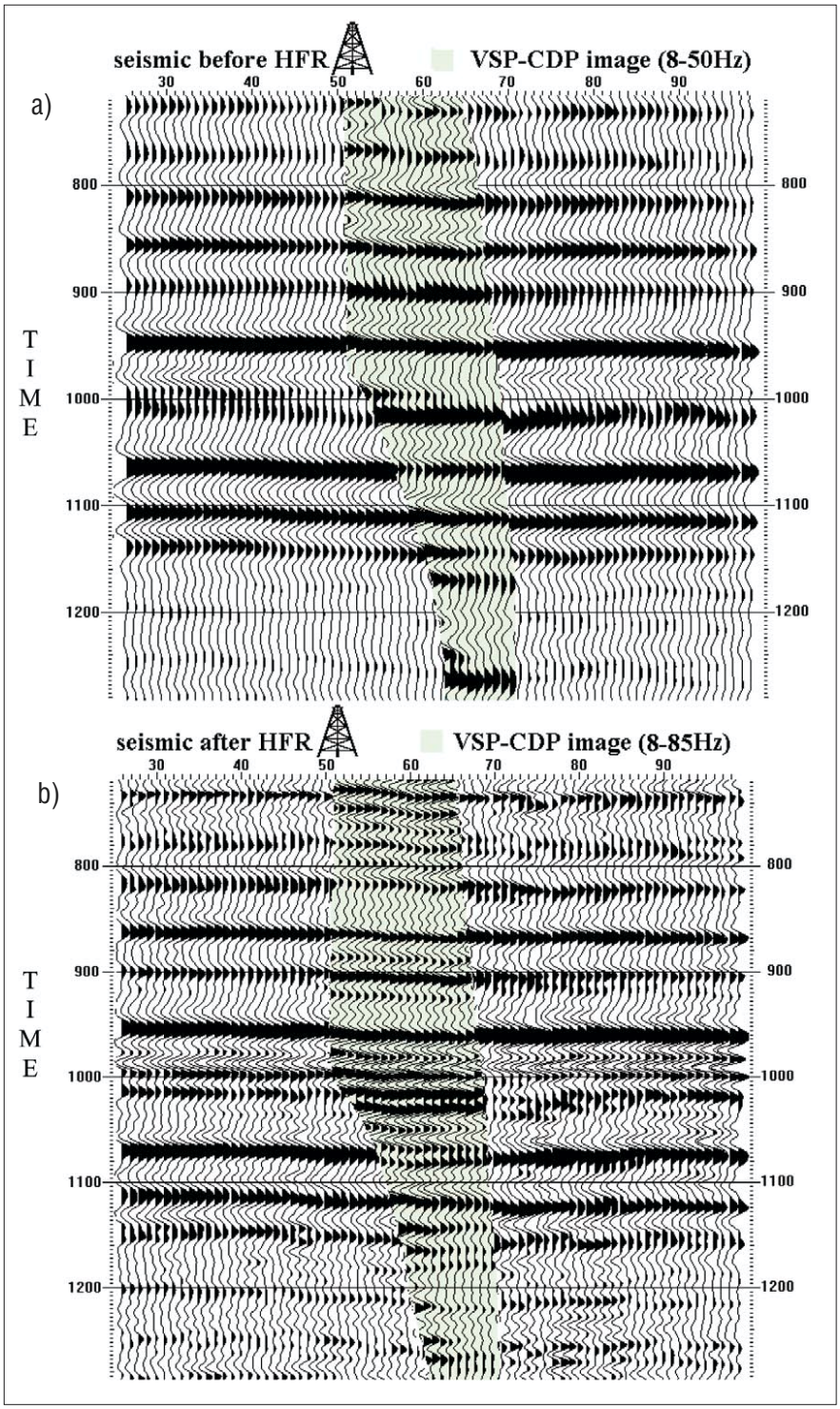


*Figure 10. Overlay of 3D VSP and seismic inline 85.*

improvement in resolution and continuity. Figure 6 indicates the extent of enhancement of the amplitude spectra. Similarly, Figure 7 shows crossline 72 before and after HFR and Figure 8 the extent of enhancement of the amplitude spectra. Reflections at levels indicated by arrows exhibit more continuity, and the match with the corridor stack is also much better at the level of interest (Figure 4). Figure 9 shows inline 85 after frequency enhancement and a comparison with the vertical section through the 3D VSP volume. There is a good correlation now between the two. Stratigraphy, VSP upgoing wavefield, and VSP corridor stack may be seen correlated with inline 85 after HFR in Figure 4.

To dispel potential doubts about the reliability of new reflection detail after HFR, we correlated the appropriate inline seismic sections with 2D vertical sections drawn from the 3D VSP volume. Figure 10a shows an offset VSP-CDP profile extracted from a 3D VSP and overlain onto inline 85 from the 3D seismic volume. The VSP profile has been bandpass filtered (8-50 Hz) to match the frequency content of the seismic data. The good matching of different reflection events is evident but the frequency bandwidth is low. Figure 10b shows the same matching after HFR. In this case, the VSP-CDP profile is filtered to 8-85 Hz. Notice the high frequency bandwidth of both the profiles and the higher level of detail available for interpretation.

**Evaluating improvement in frequency enhancement using coherence.** Time or horizon slices across coherence volumes are useful for following faults and stratigraphic features in map views, free from possible bias by interpretation. A Coherence Cube was generated on the two seismic volumes, before and after filtering, to examine the differences that are caused by HFR. In Figure 11, time slices at 984 ms, note that the patterns are more distinct and more detail is evident after filtering.

Figure 12 shows time slices at 1024 ms before and after HFR. Between wells 6-20 and 8-20, there is a low coherence trend after filtering which may explain the difference in the nature of the two wells. These trends are not so obvious on the slice before filtering.

**Impedance inversion on seismic data with higher bandwidth.** Impedance inversion performed on data with higher bandwidth yields more information than on data with poor bandwidth. For example, features that cannot be detected on seismic inversion before Q deconvolution are clearly visible after and so allow detailed interpretation of important stratigraphic features (Hirsche et al., 1984). Figure 13a shows segments of impedance sections of a 2D line (different from the data shown earlier). A gas producing well (W) is seen intersecting the highlighted portion corresponding to a gas sand. However, the green streak continues across the segment and does not distinguish the gas sand. HFR was run on the seismic section and submitted to impedance inversion (Figure 13b). Notice the dark green streak (low impedance), within the highlighted portion seen clearly representing the gas sand. This example thus amply corroborates findings similar to those of Hirsche et al. using HFR.

**Robustness of the method.** An important element that lends strong support to the utility of any procedure is robustness.

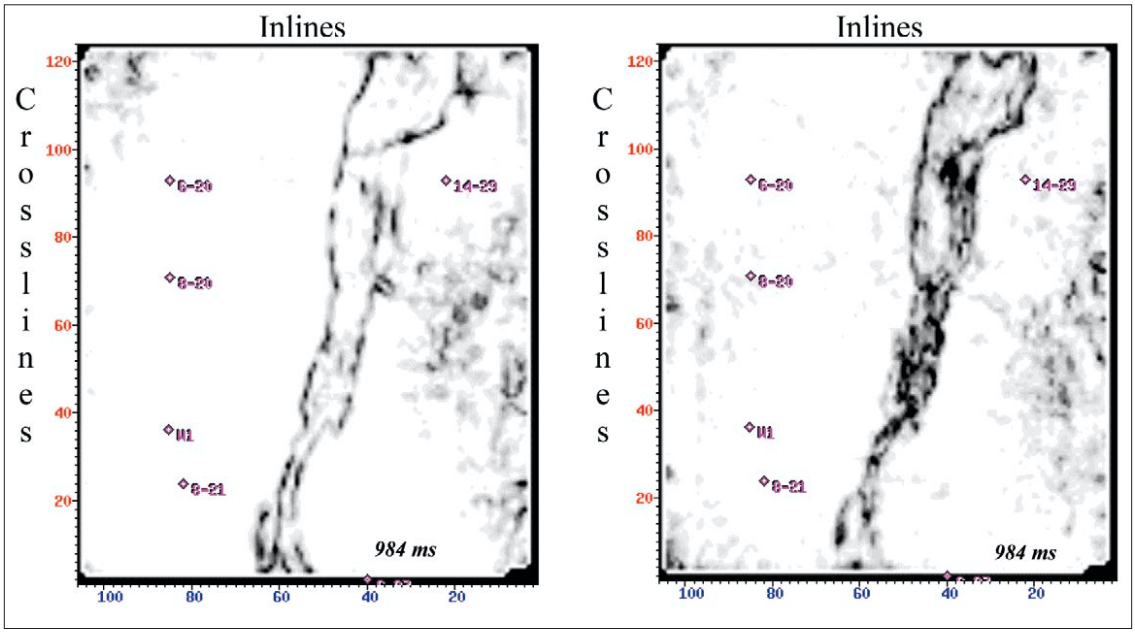


***Figure 11.*** *Time slices from the coherence volumes before (left) and after (right) HFR.*

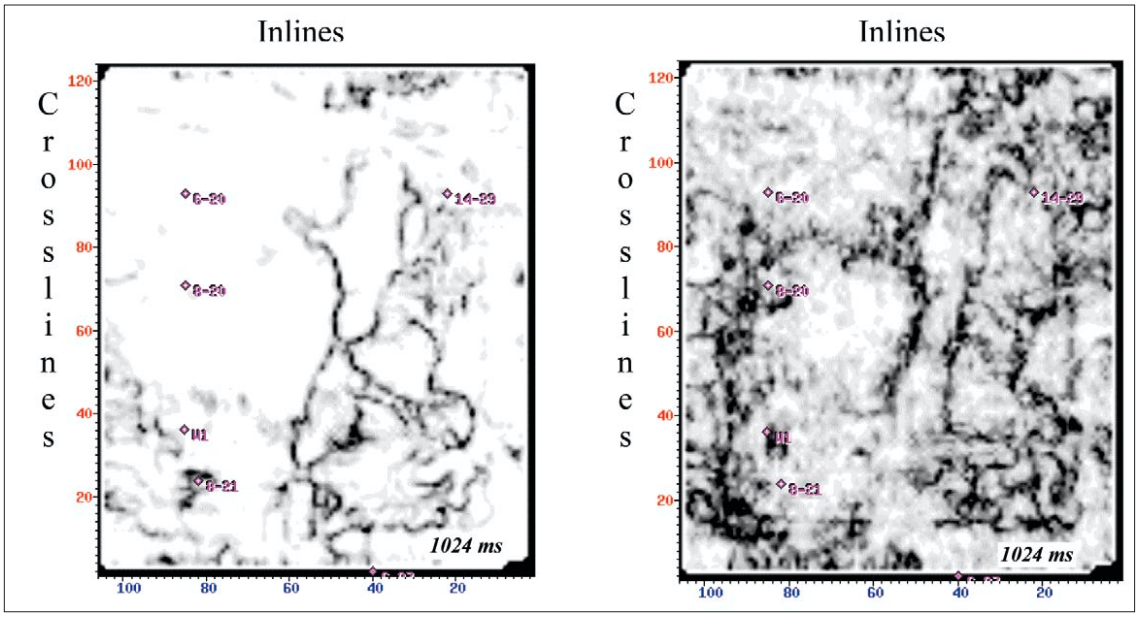


***Figure 12.*** *Time slices from the coherence volumes before (left) and after (right) HFR.*

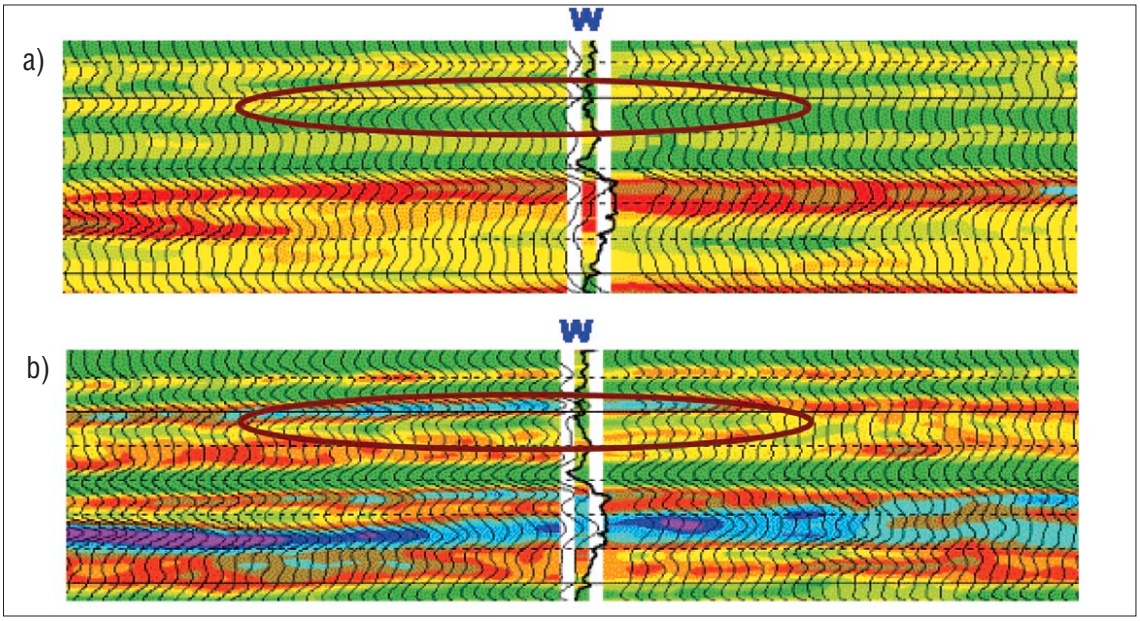


***Figure 13.*** *(a) Segment of impedance section. Highlighted portion indicates lower impedance at the level of gas sand but does not distinguish it. (b) Segment of impedance section. Highlighted portion indicates the extent of the gas sand clearly.*

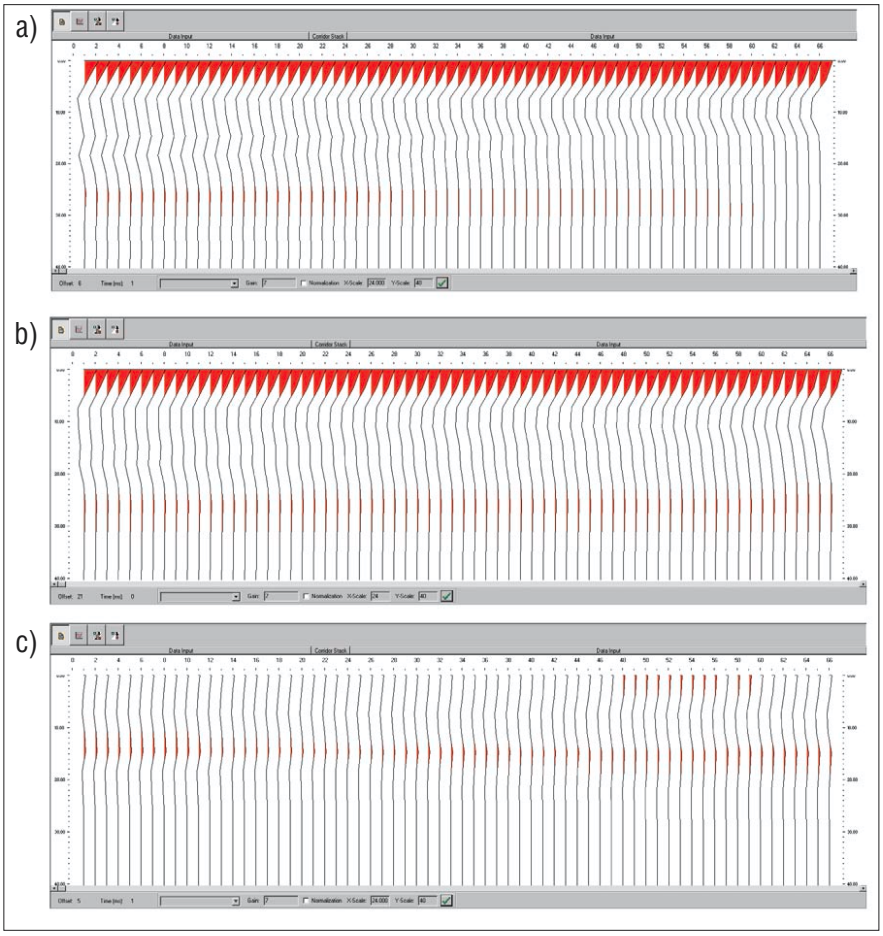


***Figure 14.*** *(a) Operators derived from well 1. (b) Operators derived from well 2. (c) Difference of operators derived from wells 1 and 2.*

For the same area, if the geology does not change abruptly, the HFR filters from different VSP surveys should be the same, (assuming data quality is good and is acquired using similar equipment). The set of inverse filters were computed from VSPs in two different wells in the same field. The objective was to determine how different these sets of filters were. Figures 14a and 14b show the filters determined from two different wells. Figure 14c shows their difference. Clearly, the filters are almost identical. Such tests carried out on different wells in different areas lead us to conclude that HFR is robust. However, in areas where geology changes fast laterally, a spatial adaptive filter application approach may be necessary.

**Prestack application of HFR.** Application of HFR to poststack data has been illustrated in the examples above. Application to prestack data is also very effective and useful for AVO analysis. However, since a zero-offset VSP is used to determine the attenuation in terms of a set of HFR filters, application to seismic gathers would mean application of the same set of filters for all offset traces. Attempts at offset-dependent correction to gathers requires several walkaway VSPs for determining one set of HFR filters for each offset. This exercise has been carried out with convincing results for AVO analysis. This work is currently under way and will be presented upon its completion.

**Conclusions.** The HFR method described in this article differs from conventional industry methods. It consists of determining the frequency-dependent decay from downgoing VSP first arrivals from successive depth levels, and then applying the inverse decay function to surface seismic data. Advantages of this procedure include:

- poor reflection zones, resulting from strong impedance contrasts above and below a particular zone of interest, show greater reflection detail and continuity and better match corridor stacks or VSP offset sections
- impedance inversion on data with HFR application, and hence higher bandwidth, show more detail and lead to more detailed interpretation of important stratigraphic features,
- HFR methodology is robust.

HFR helps define trends better and leads to more confident interpretations. Such applications could redefine prospects, which in some cases may have been declared unsuccessful, when the interpretations are based on seismic data with poor bandwidth.

**Suggested reading.** "Simultaneous acquisition of 3D surface seismic and 3D VSP data—processing and integration" by Chopra et al. (*SEG 2002 Expanded Abstracts*). "Fault interpretation—the coherence cube and beyond" by Chopra and Sudhakar (*Oil and Gas Journal*, 2000). "Azimuth based coherence for detecting faults and fractures" by Chopra et al. (*World Oil*, 2000). "Model-based Q compensation" by Hirsche et al. (*SEG 1984 Expanded Abstracts*). TLE

*Acknowledgments: Coherence Cube and HFR are trademarks of Core Laboratories. We are indebted to Bob Hardage and Rob Stewart for editing the manuscript thoroughly and improving its quality. We thank Joanne Lanteigne for formatting some images in this paper and Jan Dewar for her valuable comments and suggestions. We thank ConocoPhillips Canada for release of data and Core Laboratories for permission to publish.*

*Corresponding author: schopra@corelab.ca*